

pubs.acs.org/JACS Article

Metal—Support Interactions in Molecular Single-Site Cluster Catalysts

Benjamin S. Mitchell,[†] Andrei Chirila,[†] Jonathan A. Kephart, Andrew C. Boggiano, Sebastian M. Krajewski, Dylan Rogers, Werner Kaminsky, and Alexandra Velian*



Cite This: J. Am. Chem. Soc. 2022, 144, 18459-18469



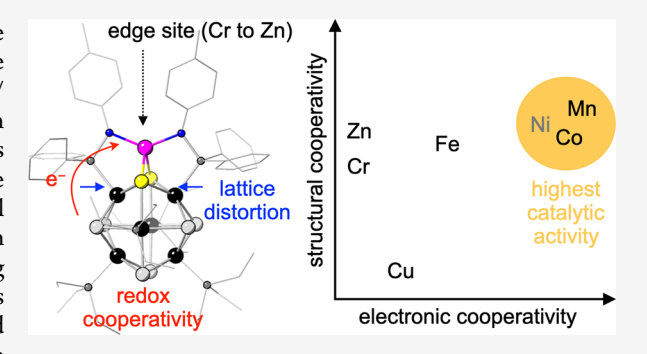
ACCESS I

III Metrics & More

Article Recommendations

s Supporting Information

ABSTRACT: This study provides atomistic insights into the interface between a single-site catalyst and a transition metal chalcogenide support and reveals that peak catalytic activity occurs when edge/support redox cooperativity is maximized. A molecular platform $MCo_6Se_8(PEt_3)_4(L)_2$ (1-M, M = Cr, Mn, Fe, Co, Cu, and Zn) was designed in which the active site (M)/support (Co_6Se_8) interactions are interrogated by systematically probing the electronic and structural changes that occur as the identity of the metal varies. All 3d transition metal 1-M clusters display remarkable catalytic activity for coupling tosyl azide and *tert*-butyl isocyanide, with Mn and Co derivatives showing the fastest turnover in the series. Structural, electronic, and magnetic characterization of the clusters was performed using single



crystal X-ray diffraction, ¹H and ³¹P nuclear magnetic resonance spectroscopy, electronic absorption spectroscopy, cyclic voltammetry, and computational methods. Distinct metal/support redox regimes can be accessed in 1-M based on the energy of the edge metal's frontier orbitals with respect to those of the cluster support. As the degree of electronic interaction between the edge and the support increases, a cooperative regime is reached wherein the support can deliver electrons to the catalytic site, increasing the reactivity of key metal-nitrenoid intermediates.

■ INTRODUCTION

Tuning metal/support interactions represents a powerful strategy to modulate catalytic activity, making supported single-site catalysts that harness these effects an active frontier of research. 1-7 The electronic and geometric interactions with the atoms of the support can critically impact the performance of the active site, particularly when the support is chemically noninnocent as is the case for transition metal chalcogenides. For instance, the coordination environment of single Rh atoms installed at edge vacancies of MoS₂ nanosheets and the charge transfer between the active sites and the support impart optimal stability and high selectivity for aldehyde hydrogenation. In a more molecularly inspired approach, tuning the number of bonds between surface-anchored Co active sites and the WS₂ nanosheet support facilitates increased activity for the electrochemical oxygen reduction. 10 More broadly, the interaction between surface or edge metal dopants and layered transition metal dichalcogenide supports has been extensively investigated in the context of identifying catalysts for industrially relevant processes, such as hydrotreatment and hydrogen evolution (Figure 1A).¹¹ In these materials, metal dopants can serve as new catalytic centers, 9,10 or alter the activity of native sites indirectly, for example by engaging in charge transfer 12-14 or by inducing structural changes within the support. 15 However, the role of the metal dopant is

complex and varies with the chemical transformation, ^{16,17} substrate identity, ¹⁸ and material morphology, ^{19–22} among other factors ^{23,24} precluding the determination of clear-cut structure—function relationships.

In contrast, coordinative noninnocence and electronic cooperativity between the ligand sphere and an active site have been extensively utilized and studied in molecular platforms. For example, systematically tuning the identity of the metals in a simplified, bimetallic platform enabled exquisite insights into the role of the supporting metal center in modulating substrate binding, activation, and catalytic performance at the active site. Extending this molecular approach to investigate constructs that embody the complexities of a heterogeneous active site could offer new perspectives for controlling catalytic activity or selectivity using metal/support interactions.

Due to their synthetic tunability and homogeneous nature, atomically precise nanoclusters are advantageous for this

Received: July 5, 2022 Published: September 28, 2022





A. Edge and surface-supported active site motifs B. Molecu redox cooperations and the surface supported active site motifs.

• transition metal • chalcogen

B. Molecular single-site cluster catalyst M edge site Cr → Zn lattice redox cooperativity

Figure 1. (A) Types of edge and surface-supported active sites on a layered transition metal chalcogenide support. (B) Single-site, atomically precise platform designed to study the electronic and structural changes at the metal/support interface, and their effects on catalytic activity.

active site

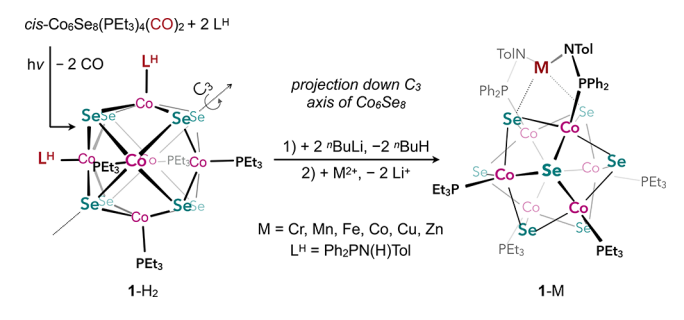
purpose and can serve as both functional models and as platforms for new catalyst development. 30,31 Examples of molecular clusters that feature metal/support architectures exist, $^{32-36}$ such as the catalytically competent $Au_n(SR)_m$ clusters in which the reactive surface gold atoms are chemically distinguished from those of the cluster core.³⁷ While tuning cluster size 38-40 and the coordination environment 41 of the active sites has been shown to modulate their catalytic activity, studies that identify the active site and systematically correlate how its identity impacts the metal/support interaction and the emerging catalytic activity are yet to materialize. To this end, our group has developed a class of nanoclusters (M3; $M_3Co_6Se_8L_6$, M = Cr, Fe, Co, Zn, and SnMe₂, L = $PPh_2N^{(-)}Tol$, Ph = phenyl, Tol = 4-tolyl) which feature three edge metals, M, anchored on the atomically precise Co₆Se₈ cluster. This construct resembles edge- and surface-metals supported on transition metal chalcogenides, but their homogeneity enables the use of molecular characterization techniques. In M3, the substrate-accessible edges facilitate not only catalytic activity 42,45 and dimensional control over nanomaterial growth, 43,44 but also provide atomic-level insights into the evolution of the active sites under catalytic conditions, and their interconnected reactivity.⁴⁵

Herein, the metal (M)/support (Co₆Se₈) interactions are interrogated by systematically probing the electronic and structural changes that occur at this interface as the identity of the metal varies in the 3d period. The role of the metal/ support cooperativity in modulating reactivity is explored in the context of catalytic nitrene transfer. To this end, a singlesite cluster platform $MCo_6Se_8(PEt_3)_4(L)_2$ (1-M, M = Cr, Mn, Fe, Co, Cu, and Zn) was designed to (i) circumvent the complexities of multi-site dynamics present in M3, and (ii) enable systematic modification of the edge metal identity (Figure 1B). This study reveals that distinct metal/support redox regimes can be accessed in 1-M based on the energy of the edge metal's frontier orbitals with respect to those of the cluster support. As the degree of electronic interaction between the edge and the support increases, a cooperative regime is reached wherein the support can deliver electrons to the catalytic site, increasing the reactivity of key metal-nitrenoid intermediates. By using a cluster as a support, this work provides an atomic-level picture into how these effects manifest in a heterogeneous single-site catalyst, and illustrates how metal/support interactions can be used to facilitate catalysis.

■ SYNTHESIS OF SINGLE-SITE CLUSTERS 1-M

Site-differentiation of a cluster with chemically degenerate surface sites is a challenging synthetic pursuit. Successful strategies to accomplish this include stoichiometric control of reagents, ^{47–50} engineering sophisticated or very bulky ligand frameworks, 32,51,52 or by relying on allosteric effects between multiple edge sites.⁴⁴ Here, the synthesis of clusters with a single active site relies on access to isomerically pure samples of the site-differentiated cluster cis-Co₆Se₈(PEt₃)₄(CO)₂ in which two carbonyl groups localized on cis-cobalt sites can be precisely displaced by nucleophiles without scrambling on the cluster surface. 49 Photolysis of the cis-carbonyl cluster in the presence of excess aminophosphine Ph₂PN(H)Tol (L^H) results in the formation of cis-Co₆Se₈(PEt₃)₄(L^H)₂ (1-H₂; 84% isolated yield; Scheme 1). The metalloligand 1-H₂ features one well-defined binding site poised to anchor a single metal to the surface of the Co₆Se₈ support via amide chelation and up to two hemilabile M-Se interactions. Deprotonation of the aminophosphines of $1-H_2$ with nbutyllithium and subsequent treatment with the salt of a divalent metal ($M^{2+} = Cr^{2+}$, Mn^{2+} , Fe^{2+} , Co^{2+} , Cu^{2+} or Zn^{2+}) leads to the formation of a single new species identified as the monometallated cluster MCo₆Se₈(PEt₃)₄(L)₂ (1-M; 71-96% yield). With the exception of 1-Cr(Sol) (Sol = tetrahydrofuran (THF), py), the monometallated clusters are isolated without bound exogenous ligands, which is in contrast to their trimetallated counterparts, typically isolated as solvent adducts $M_3(Sol)_x$ (M = Cr, Fe, Co, Zn) despite their identical coordination environment at M. $^{42-45}$ This apparent lower affinity for ligands is likely a consequence of the more electron rich Co₆Se₈ core in the 1-M series, 53 which features just one Lewis acidic metal on its surface, and four electron donating triethylphosphine groups.

Scheme 1. Synthesis of Single-Site Clusters



■ TRENDS IN CATALYTIC ACTIVITY

Transition metal catalyzed N-group transfer is an attractive method to selectively and efficiently form carbon-nitrogen bonds. ^{54,55} We previously discovered that Fe₃ and Cr₃(py)₃ are excellent catalysts for the coupling of tosyl azide (TsN₃) and *tert*-butyl isocyanide ([†]BuNC) to form the asymmetric carbodiimide TsNCN[†]Bu, therefore this transformation was used to benchmark the relative reactivity of the 1-M series. Here, we discovered that all of the monometallated clusters catalyze this transformation at room temperature with 1 mol % catalyst loading, whereas 1-H₂ shows negligible activity (Figures 2 and S30). Inspecting the kinetic profiles of the

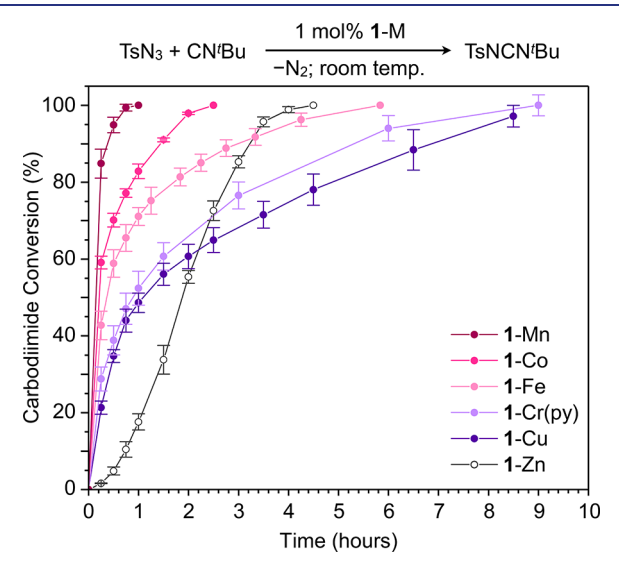


Figure 2. Catalytic conversion of carbodiimide (TsNCN^tBu) with 1 mol % loading of 1-M cluster. Conversion determined by ¹H nuclear magnetic resonance (NMR) integrations of the product and reactants.

homologues, 1-Mn stands out as the most efficient catalyst with 50% conversion $(t_{1/2})$ achieved in just 5 min followed by 1-Co (10 min), 1-Fe (22 min), 1-Cr(py) (53 min), and 1-Cu (66 min), respectively. In contrast to the other clusters, the conversion profile of 1-Zn features a slow induction period followed by a very active catalytic regime, suggesting a different catalytic pathway is at play than in the other clusters, likely associated with a loss of structural integrity of the Zn/Co₆Se₈ construct. To assess the stability of the 1-M clusters during this transformation, we analyzed the postcatalytic reaction mixtures using ¹H NMR spectroscopy at 10% 1-M loading (Figure S32). Under these conditions, 1-Co is completely regenerated. Although only ca. 60% of 1-Fe is recovered upon substrate depletion, the remaining 40% is accounted for by the formation of a single new species, ostensibly the iron amido complex 1-Fe(NHTs) (Figure S31). Some cluster fragmentation likely occurs for 1-Zn and 1-Cu where NMR analysis indicates that the resulting reaction mixture contains multiple unidentified species in addition to some recovered 1-M cluster (17 and 23%, respectively). The spectroscopic analysis of the 1-Cr and 1-Mn samples does not suggest cluster degradation, but the broad, paramagnetic features of these clusters make quantitative NMR analysis unreliable. While an extensive investigation into the speciation of the clusters under catalytic conditions is beyond the scope of this study, we point out that the trimetallated derivatives Fe_3 and $Cr_3(py)_3$ catalyze this transformation without any observable cluster decomposition. 42,45 Carbodiimide formation typically occurs via the formation of metal-nitrenoid intermediates. $^{54,56-58}$ The recent isolation of catalytically competent metal-imido nanocluster intermediates (e.g., $Cr_3(NTs)_3$) demonstrated this is the case for the chromium derivative, confirming that the three edge sites are indeed catalytically active and that the edge/support construct is viable under catalytic conditions. 45

STRUCTURAL ANALYSIS

Single crystal X-ray diffraction analysis of the 1-M cluster series reveals that three different coordination geometries can be distinguished at the edge sites depending on the chemical identity of M (Figure 3A,B). The Mn, Fe, Co, and Zn edges feature distorted tetrahedral geometries, and are chelated κ^4 by the cluster via two amides and two Se atoms. Although the Ni congener has proven challenging to isolate experimentally, its geometry and electronic structure were modeled in silico and found to adopt a similar pseudotetrahedral edge coordination (Section S8). In the Cr variant, characterized in the solid state as a THF adduct, the edge site features a pseudosquare pyramidal geometry similar to that observed for the trimetallated analogue Cr₃(py)₃, with one short and one long Cr-Se bond (2.581(6) and 2.772(7) Å). In contrast, the edge site does not engage in bonding with Se in 1-Cu (Cu...Se > 2.792(5) Å). The nearly linear N-Cu-N bond angle of $172.5(1)^{\circ}$ is a mark of Cu¹⁺ and suggests that upon metallation with the Cu²⁺ salt an intramolecular electron transfer occurs between the edge and the support that gives rise to a Cu¹⁺/ Co₆Se₈¹⁺ complex. A contraction in the Co...Co distances within the Co_6Se_8 core, typically associated with mono-oxidation, is indeed observed in 1-Cu (Figure 3C). Electrochemical, magnetic, and NMR data, as well as density functional theory (DFT) analysis also support this interpretation, as discussed in later sections. Monometallation gives rise to systematic distortions within the Co₆Se₈ core (Figure 3C and Table S5). These are primarily localized at the MCo₂Se₂ edge where the most striking change brought upon installing the edge site is an increased interatomic separation of the two Se atoms. The MCo₂Se₂ edge features elongated Co-Se bonds and contracted Co...Co distances compared to the rest of the Co₆Se₈ core, where the distortion trends are reversed such that overall the average metrics of the nonmetallated clusters (i.e., Co₆Se₈L^H₆ and Co₆Se₈(PEt₃)₄(CO)₂) are preserved under comparison of the M...Se interatomic distances in the 1-M series to the average distance for the M-Se single bond in the Cambridge Structural Database, suggesting that the edge metal is bound strongest to the Se in the Mn and Co derivatives followed by the Cr, Fe, and Zn complexes, whereas no Cu...Se bonding interactions are present in 1-Cu. 60-62

■ ELECTRONIC STRUCTURE INVESTIGATIONS

The magnetic response of the 1-M nanoclusters was probed by solution phase magnetic susceptibility measurements using the Evans method. The parent 1-H₂ cluster is diamagnetic, and remains closed-shell upon monometallation with zinc. 1-Cr(py), 1-Mn, 1-Fe, and 1-Co are paramagnetic with effective magnetic moments of 4.6(3), 5.4(3), 4.9(3), and 3.8(3) $\mu_{\rm B}$, respectively, close to those expected for high-spin M²⁺ edge sites with S = 2, 5/2, 2, and 3/2. The high-spin state of the edge metals in 1-Mn, 1-Fe, and 1-Co is consistent with the pseudo-tetrahedral coordination environment enforced by the cluster support, and is in agreement with earlier investigations

C. Structural distortions at the MCo₂Se₂ edge A. Structural characterization of the 1-M clusters Se...Se expansion Co...Co Co contraction edge i) Se...Se 3.5 core ii) Co...Co 1-Cr(THF) **1**-Mn **1**-Fe edge core iii) Co-Se edge core iv) M-Se Δ vs CSD 0.0 CSD avg 15 1-Co 1-Cu **1**-Zn B. Structural variations in the coordination of the edge metal Co edge Cr edge Mn edge Fe edge Cu edge Zn edge 01 N2 N2 N2 N₃ N2 N4 N₁ Se1 Se10 Se₁₀ Se1 Se9 b Se2 Se2 Se1 Se1 Se2 @ Se9

Figure 3. (A) Single crystal X-ray structure of 1-Cr(THF), 1-Mn, 1-Fe, 1-Co, 1-Cu, and 1-Zn. Ellipsoids are plotted at 50% probability, and carbon backbones are depicted as wireframes. Disorder, hydrogen atoms, and co-crystallized solvent molecules are omitted for clarity. (B) Zoom-ins on the first coordination sphere of the edge sites. (C) (i-iii) Edge (MCo₂Se₂) and core (Co₆Se₈) structural distortions upon monometallation. (iv) Deviation of the two M-Se interatomic distances from the average M-Se value reported in the Cambridge Structural Database.

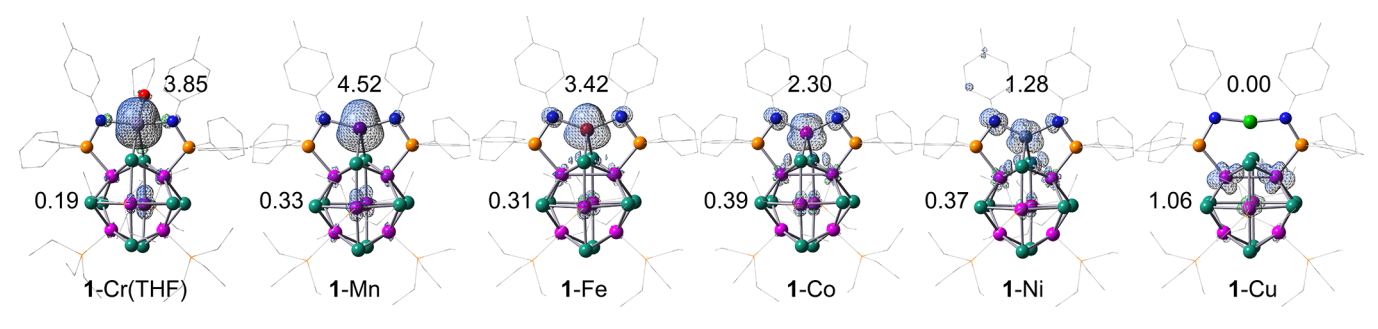


Figure 4. Mulliken spin density $(\alpha - \beta)$ plots of 1-M series calculated at the DFT uB3LYP+/cc-pVTZ level of theory. Spin density values for the edge "M" and Co₆Se₈ core are included. Surfaces plotted at an isovalue of 0.004.

into the electronic structure of Fe₃ and Co₃(py)₃ reported by our group. 42,43,53 DFT calculations predict that while most of the spin (64-90%) is localized on the edge metal's 3d orbitals in 1-Cr(py), 1-Mn, 1-Fe, 1-Co, and 1-Ni, there is a contribution from the cobalt core (5-19%) which indicates some spin mixing between the paramagnetic edge metals and the Co₆Se₈ support (Figure 4, Table S6).⁶⁵ In contrast, the entirety of the spin density calculated for 1-Cu is localized on the Co₆Se₈ support, which is in line with the proposed

redistribution of charge between the edge and support that results in a diamagnetic Cu^{1+} site and a mono-oxidized S = 1/2[Co₆Se₈]¹⁺ cluster core. Experimentally, 1-Cu has an effective magnetic moment of 1.8(3) $\mu_{\rm B}$, which cannot be used to distinguish between Cu1+/[Co6Se8]1+ and Cu2+/[Co6Se8]0. It is interesting to note that the predicted distribution of the unpaired electrons in 1-Cu is not uniform in the cluster core but is concentrated on the cobalt centers closest to the copper edge site. The localization of lattice distortion and spin closest

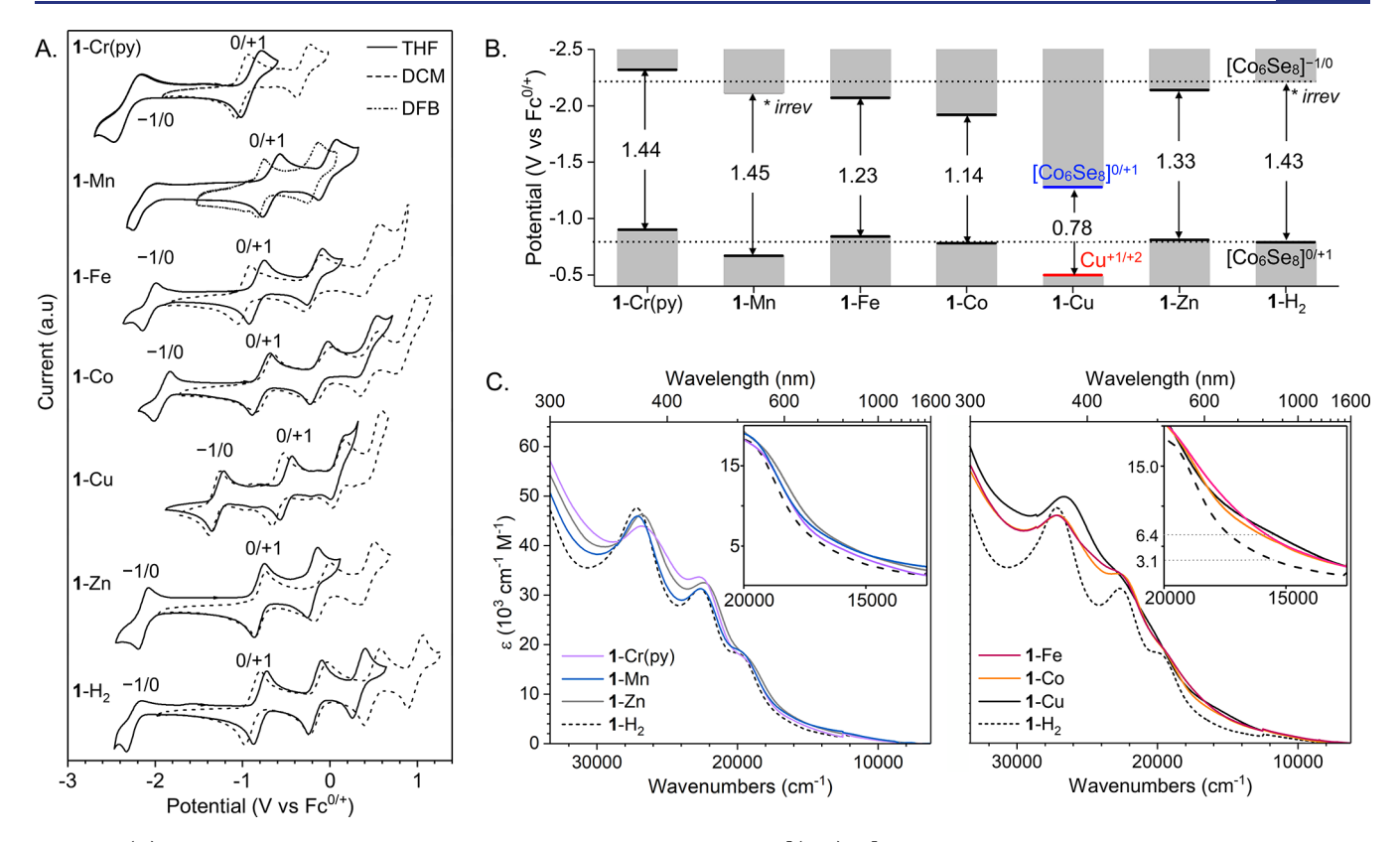


Figure 5. (A) Cyclic voltammograms of 1-M series recorded in 0.1 M solutions of $[("Bu)_4N]PF_6$ in THF, dichloromethane, or 1,2-difluorobenzene at a scan rate of 200 mV/s and referenced to the ferrocene/ferrocenium redox couple. (B) Relative potentials of the highest occupied molecular orbital (HOMO)/lowest-unoccupied molecular orbital (LUMO) levels for each of the homologues in the 1-M series, estimated from the 0/+1 and 0/-1 events in THF. (C) Electronic absorption spectra collected in THF for the 1-M series (left, M = Cr(py), Mn, Zn; right, M = Fe, Co, and Cu) plotted versus the spectrum of 1-H₂. Insets feature zoom-ins of the absorption in the visible and near-infrared (IR) range. Extinction coefficient of 1-Co was not measured.

to the edge site mirrors experimental observations and theoretical models for the interfacial perimeter in heterogeneous metal/support constructs.⁴

Electronic absorption spectroscopy and electrochemical measurements reveal that the electronic interaction between the edge and core is the greatest in 1-Fe, 1-Co, and 1-Cu, whereas metallation with Cr, Mn, and Zn does not perturb the electronic structure of the metalloligand 1-H2 significantly (Figure 5). In 1-Fe, 1-Co, and 1-Cu, the three characteristic ultraviolet absorption bands of the Co₆Se₈ core broaden, and the absorption in the visible and near IR spectral range intensifies significantly. For example, at 650 nm, the 1-Cu derivative has an absorption coefficient of 6400 cm⁻¹ M⁻¹, more than double that of 1-H₂ (Figure 5C). Similar, but more pronounced electronic changes associated with edge/core interactions have been observed in the trimetallated analogues. 42 The increased absorption in the visible and IR range indicates decreased HOMO/LUMO gaps, which is corroborated by electrochemical analysis (Figure 5A). In contrast, the electronic absorption spectra of 1-Cr(py), 1-Mn, and 1-Zn trace closely with that of 1-H₂, with only a very small redshift in the absorption (<5 nm) suggesting these metals have minimal influence on the electronic structure of the cobalt core.

Electrochemical analysis reinforces the trends observed in the optical spectra (Figure 5A,B). Cyclic voltammetry reveals that monometallation induces a narrowing of the HOMO/LUMO gap in 1-Fe, 1-Co, and especially in 1-Cu, whereas in

1-Zn, 1-Cr(py) and 1-Mn it remains nearly identical to that of 1-H₂. Here, the HOMO/LUMO gaps are estimated from the energetic difference between the first oxidation and first reduction events in THF. Overall, the 1-M clusters retain rich redox profiles that are reminiscent of the metalloligand 1-H₂ itself featuring four chemically reversible one-electron oxidations and one irreversible reduction. Notably, upon metallation, the first reduction becomes chemically reversible for all derivatives except 1-Mn and is stabilized in the series Mn < Fe < Co \ll Cu.

Overall, the effect of monometallation on the electronic structure is proportional to the extent of structural distortion the edge site inflicts on the Co/Se cluster (Figure 3C). Thus, little electronic and structural distortions are observed for 1-Cr, whereas in 1-Fe and 1-Co the decreased HOMO/LUMO gaps and redshift in the electronic absorption compared to 1-H₂ are accompanied by pronounced structural distortions and increased M–Se interaction strength. Exceptions to this trend are the d^5 and d^{10} derivatives 1-Mn and 1-Zn, which feature structural distortions and relatively short M–Se bonding interactions but have HOMO/LUMO gaps and electronic absorption spectra resembling those of the parent ligand.

■ PARAMAGNETIC ³¹P NMR SPECTROSCOPY REPORTS ON THE ELECTRONIC STRUCTURE

The chemically differentiated phosphines in 1-M make them excellent reporters on the local electronic microenvironments.

The ^{31}P NMR chemical shifts of the triethylphosphine ligands capping four of the six cobalt sites in Co_6Se_8 report directly on the support. The amidophosphines cap the remaining two cobalt centers in the cluster, but also directly anchor the surface metal, therefore informing on both the edge and the support.

While no 31 P NMR signals were detected for the Cr and Mn derivatives, 1-Fe, 1-Co, 1-Cu, and 1-Zn display diagnostic chemical shifts. The observed experimental chemical shift of a paramagnetic compound $(\delta_{\rm T}^{\rm obs})$ is the sum contribution of the diamagnetic $(\delta^{\rm dia})$ and paramagnetic $(\delta_{\rm T}^{\rm para})$ components of which only the latter is temperature (1/T) and spin dependent (eq S1). The diamagnetic 1-Zn cluster has chemical shifts similar to those of the free ligand. Meanwhile, the paramagnetic variants reveal a linear dependence of the 31 P NMR chemical shifts with the inverse of temperature (Figure 6). As

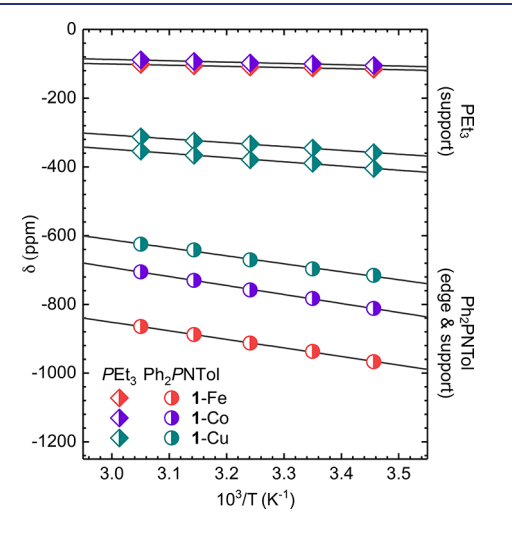


Figure 6. Curie behavior of 1-Fe, 1-Co, and 1-Cu reflected in the linear dependence of the ³¹P NMR chemical shifts with an inverse temperature in the 290 to 330 K range.

the spin state of the clusters increases in the 1-Cu (S=1/2), 1-Co (S=3/2), and 1-Fe (S=2) series, the ³¹P chemical shifts associated with the amidophosphine become more negative (-663, -796, and -956 ppm, respectively). Spatially removed from high-spin edge metals, the chemical shifts of the PEt₃ capping ligands are very similar for 1-Fe and 1-Co (-113 and -98 ppm, respectively) where the Co₆Se₈ core is expected to stay diamagnetic. In contrast, they shift dramatically in 1-Cu (-354 and -400 ppm), corroborating our hypothesis that the cluster core is mono-oxidized (S=1/2). While the $C_{2\nu}$ cluster symmetry gives rise to two distinct PEt₃ environments in 1-M, these are only resolved by ³¹P NMR spectroscopy for the 1-Cu derivative. We attribute this to the localization of the charge on the cobalt atoms proximal to the edge site, as predicted by DFT (Figure 4).

CALCULATED ELECTRONIC STRUCTURES

DFT calculations carried out at the uB3LYP+/cc-pVTZ level of theory closely reproduce the structural and electrochemical experimental data of 1-M (Figures S54).^{69–72} Considering the large number of electronic states, the energetic overlap and relative contributions of the edge and core atoms to the valence orbitals and lowest energy unoccupied levels in the 1-M clusters are more clearly visualized using density of states plots.⁷³ Inspecting Figure 7, we note that the energy of the d orbitals decreases in the atomic series Cr, Mn, Fe, Co, and Ni. 12,74,75 This manifests at the LUMO levels where the edge metal contribution increases across the series, eventually peaking at Ni, where the first reduction is predicted to be primarily nickel, not Co_6Se_8 -centered. The predicted increase in the edge metal contribution at the LUMO level correlates directly with the lowering in energy observed experimentally for the 0/-1 electrochemical reduction (Figure 5A). As expected, the calculations reveal that there is no contribution to the LUMO levels from the d¹⁰ Zn²⁺ and Cu¹⁺ edges. 1-Cu is electronically different from the rest of the series. Corroborating the structural, magnetic, NMR, and electrochemical data, DFT calculations predict that the HOMO level is localized on

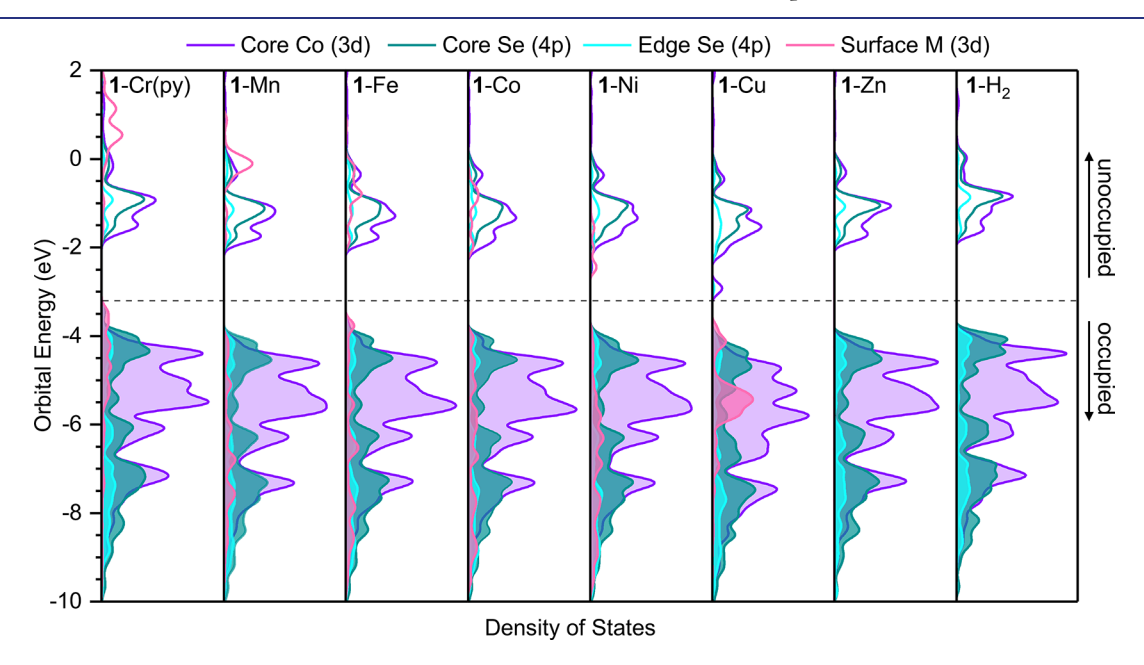


Figure 7. Partial density of states plots of 1-M series calculated at the uB3LYP+/cc-pVTZ level of theory.

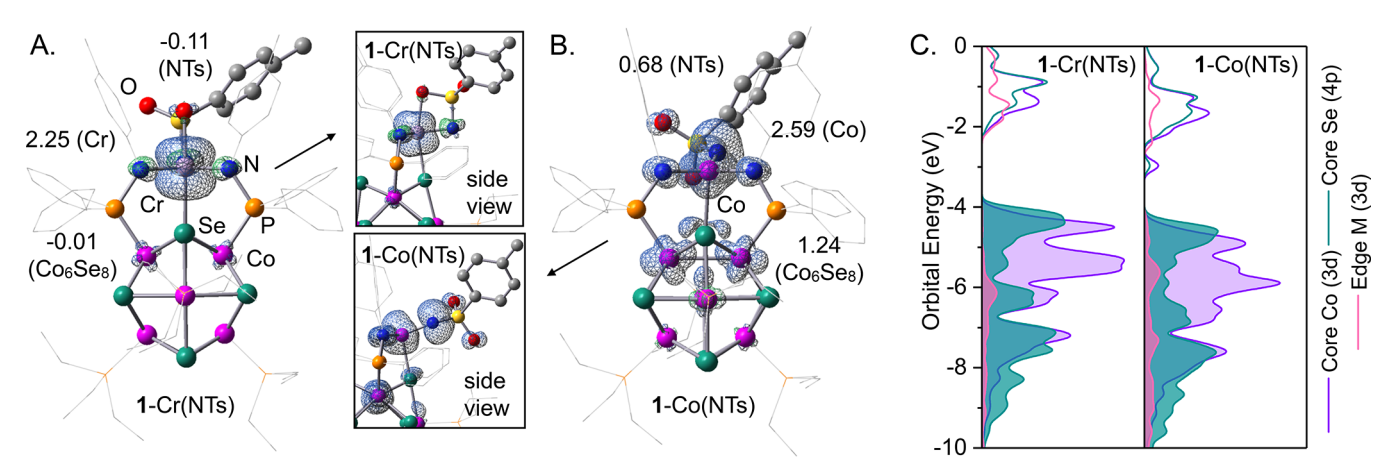


Figure 8. Mulliken spin density $(\alpha-\beta)$ plots of (A) 1-Cr(NTs) and (B) 1-Co(NTs) calculated at the uB3LYP+/cc-pVTZ level of theory. Spin density values for the edge, NTs fragment, and Co₆Se₈ core are included. Surfaces plotted at an isovalue of 0.004. (C) Corresponding partial density of states plots of 1-Cr(NTs) and 1-Co(NTs).

the Cu^{1+} edge site. Additionally, they reveal that the low-lying LUMO level is associated with the mono-oxidized core $[\text{Co}_6\text{Se}_8]^{1+}$, explaining the markedly lower 0/-1 reduction potential measured for 1-Cu.

DECONSTRUCTING EDGE/CORE COOPERATIVITY: METAL/SUPPORT INTERACTION STRENGTH AND REDOX REGIMES

The Co₆Se₈ cluster core ostensibly modulates the reactivity of the edge site by engaging in hemilabile edge-Se interactions on demand, or by providing electrons (or holes) to the reaction site. Empirically, the strength of the edge/core interaction in the 1-M precatalysts is found to track linearly with the catalytic activity, such that the species with the shortest M-Se bonds in the solid state are also the most active catalysts (1-Mn > 1-Co > 1-Fe > 1-Cr > 1-Cu). This apparent trend in reactivity is illustrated in Figure S53 where the deviation of the edge M-Se bond lengths from the corresponding average values extracted from the Cambridge Structural Database, $^{60-62}$ is plotted against the observed catalytic activity for carbodiimide formation. We hypothesize that as the edge/support (M-Se) interaction becomes stronger, the edge/nitrenoid (M-NTs) interaction weakens thereby becoming more reactive. Earlier studies into the trimetallated M₃ nanoclusters corroborate this claim by revealing a strong interdependence in the substrate/edge site/support interaction dynamics. 42,44 For example, in the trichromium nanocluster Cr3, a catalyst for carbodiimide formation, edge sites that engage in stronger Cr-Se bonding interactions with the support form weaker edge/substrate (Cr-NTs) interactions, 45 although for this system the kinetic implications of this coordinative interplay could not be separated from isocyanide binding equilibria at the Cr(NTs) edge. In the 1-M series, isocyanide binding is low for Zn, Cu, and Fe, intermediate for Mn and Co, and high for Cr, however, since the mechanism and rate-determining step for each of these species is expected to vary, extracting direct correlations to catalytic activity is tenuous (Section S6). Ultimately, it is important to note that this trend in reactivity (Mn > Co > Fe > Cr > Cu) could also reflect the intrinsic periodic differences in the reactivity of the 3d edge metal. For example, experimentally determined bond dissociation energies for metal-oxo fragments, isoelectronic with the putative metalnitrenoid intermediates in azide activation, also increase in the series Mn < Co < Fe < Cr. 76

The redox activity of the cobalt selenide support positions it to become electronically involved during a multielectron transformation such as azide activation and nitrene transfer, modulating the reactivity of the edge site. To identify the distinct regimes of edge/support redox cooperativity as a function of edge site identity, the calculated electronic structures of 1-M were used to assess which derivatives energetically favor redox cooperativity. When M = Cr or Fe, the HOMO level is predicted to be primarily localized on the edge site, suggesting the cluster core is minimally involved with oxidation. When M = Cu, the edge metal has low-lying empty orbitals to which the core spontaneously transfers an electron, reducing the edge site. As in the case of Cr and Fe, here, the first oxidation is expected to be localized strictly on the edge metal (Cu¹⁺), with no cluster core participation. Finally, when M = Co, Mn, and Ni, the similar energy of the edge atom and Co/Se core orbitals at the HOMO level positions the core to become electronically involved and, together with the strong M-Se interactions, facilitates edge/core charge redistribution during a redox reaction. This redox cooperative regime is empirically associated with the most active catalysts, 1-Co and 1-Mn. Its implications for the electronic structure of the metalnitrenoid intermediate are explored below and contrasted with the scenario in which the edge site is redox independent from the cluster core.

■ ROLE OF EDGE/CORE ELECTRONIC INTERACTIONS IN MODULATING M—N MULTIPLE RONDS

To evaluate the role of the edge/support cooperativity in modulating the reactivity of 1-M, the electronic structure of two metal-nitrenoid intermediates, ostensibly the key intermediates in azide activation and nitrene transfer, was investigated in silico. Two clusters were selected to illustrate the distinct regimes of electronic edge/support interactions, 1-Cr(NTs) in which the Cr edge site is expected to be redox independent of the cluster core, and 1-Co(NTs) in which the cobalt core is poised to become electronically involved. Electronic structure calculations of 1-Cr(NTs) (S = 1) reproduce the experimental metrics for Cr(NTs) edge sites in the previously isolated Cr_3 nanocluster system (Table S7), 45

and indicate that upon azide activation the oxidation is indeed localized on the chromium edge. This is reflected in the density of states plot of 1-Cr(NTs) by the large Cr contribution at the LUMO levels, and the exclusive Co₆Se₈ contribution at the HOMO frontier levels (Figure 8C). Spin density plots reveal that the resulting Cr4+-imido confines the unpaired spin on the Cr edge, while the cobalt selenide core remains largely unaffected (Figure 8A,B).

In contrast to the edge/support redox independence in 1-Cr, calculations suggest that the Co₆Se₈ support contributes an electron to activating tosyl azide in 1-Co. The resulting 1-Co(NTs) (S = 5/2) cluster features a Co^{2+} -iminyl edge on a mono-oxidized [Co₆Se₈]⁺, whereas a Co³⁺-iminyl might be expected in the absence of the cluster core participation. The density of states plot of 1-Co(NTs) reveals the LUMO level is completely localized on the Co₆Se₈ core, while the Co edge metal contributes to the HOMO levels (Figure 8C). Metal-nitrenoid Cr, 58,77,78 Mn, 79,80 Fe, 81–84 Co, 85–88 Ni, 89–91 and Cu^{92,93} species exist in a variety of electronic configurations, ^{56,94} and while no Co²⁺-iminyl has yet been isolated, one has recently been implicated.⁹⁵ In general, metal centers with high oxidation states and low spin configurations impart stability to a metal-nitrenoid fragment. In contrast, lower oxidation states and high-spin intermediates as those likely at play in 1-Co are more reactive due to the population of antibonding orbitals and the increased electron-electron repulsion both of which destabilize and weaken the M...N bond. We therefore hypothesize that when M = Co, the cluster core localizes some of the charge created upon N₂ extrusion (+1), enabling the edge metal to retain a relatively lower oxidation state. In turn, this Co²⁺-iminyl electronic structure is expected to feature a decreased bond order, and hence display higher reactivity. 94 Thus, in the case of 1-Co, the edge/support cooperativity is poised to increase the reactivity of the M-NTs multiple bond fragment.

CONCLUSIONS

1-M is a molecular cluster that incorporates complexities of a heterogeneous single-site catalyst in a tunable and monodisperse platform. Leveraging a molecular approach, this study provides atomistic insights into the metal/support interface, and how the ensuing cooperativity can be harnessed to enhance catalytic activity in a redox transformation.

As a ligand, the Co₆Se₈ cluster is structurally and electronically responsive to the chemical identity of the edge site. The structural versatility is captured by the variety of coordination environments adopted by the edge metals in the solid state: two coordinate linear (Cu), four-coordinate pseudo-tetrahedral (Mn, Fe, Co, and Zn), or five-coordinate square pyramidal (Cr). The electronic effects of the metal/ support interactions are probed by cyclic voltammetry, magnetic measurements, electronic absorption spectroscopy, paramagnetic ³¹P NMR, and DFT calculations. The most obvious change observed is the narrowing of the HOMO/ LUMO gaps, which is proportional to the degree of structural distortion inflicted by the edge site on the Co₆Se₈ cluster. Periodic trends in the valence orbital energies across the 3d series manifest in a stabilization of the LUMO levels across the 1-M series up to copper, where edge/support charge redistribution occurs spontaneously to form a reduced Cu1+ edge and a mono-oxidized to [Co₆Se₈]⁺ core. Ultimately, the use of molecular characterization techniques provides an atomic-level picture of the edge/cluster interface.

Metal/support interactions have been shown to enhance the catalytic activity of single-site heterogeneous catalysts. In 1-M, the edge/support construct imparts remarkable activity for nitrene transfer across the 3d transition metal series, chemical versatility that is reserved to few molecular ligands. 98,99 The identity of the edge metal effectively tunes the observed catalytic rates, which peak for the Mn and Co derivatives. Empirically, the strength of edge/core (M-Se) bonding interaction correlates linearly with the catalytic activity of the 3d series. We hypothesize that due to dynamic push-pull substrate/active site/support interactions, the strength of the M-Se bonds and M-NTs multiple bonds is inversely related. Hence, the stronger the edge/core interaction, the weaker and more reactive the M(NTs) fragment in key metal-nitrenoid catalytic intermediates. Identifying redox regimes wherein electronic cooperativity can occur between the active site and the cluster support provides a method to tune the reactivity of metal-ligand multiple bonds. The electronic interaction between the edge metal and the cluster support ranges from fully independent (Cr) to cooperative (Co, Mn). In the latter, electron transfer from the cluster core to the edge site is predicted to increase the reactivity of the metal-nitrenoid intermediate by ensuring a relatively lower oxidation state of the active site and weakening the M(NTs) bond.

In aggregate, this study provides an atomic-level picture into the key structural and electronic factors underpinning metal/ support interactions and their role in facilitating reactivity in a molecular single-site cluster, ultimately illustrating how their cooperativity can be leveraged to modulate catalytic performance.

ASSOCIATED CONTENT

Supporting Information

The Supporting Information is available free of charge at https://pubs.acs.org/doi/10.1021/jacs.2c07033.

DFT geometry optimized coordinates (TXT)

Synthetic protocols and experimental characterization for all compounds including crystallographic data, catalytic nitrene transfer studies, isocyanide binding affinity studies, and computational investigations (PDF)

Accession Codes

CCDC 2113026-2113031 contain the supplementary crystallographic data for this paper. These data can be obtained free of charge via www.ccdc.cam.ac.uk/data_request/cif, or by emailing data request@ccdc.cam.ac.uk, or by contacting The Cambridge Crystallographic Data Centre, 12 Union Road, Cambridge CB2 1EZ, UK; fax: +44 1223 336033.

AUTHOR INFORMATION

Corresponding Author

Alexandra Velian - Department of Chemistry, University of Washington, Washington 98195, United States; orcid.org/0000-0002-6782-7139; Email: avelian@ uw.edu

Authors

Benjamin S. Mitchell – Department of Chemistry, University of Washington, Washington 98195, United States; orcid.org/0000-0001-6585-2237 Andrei Chirila - Department of Chemistry, University of

Washington, Washington 98195, United States; orcid.org/0000-0001-9657-2334

- Jonathan A. Kephart Department of Chemistry, University of Washington, Washington 98195, United States;
 orcid.org/0000-0003-4608-1160
- **Andrew C. Boggiano** Department of Chemistry, University of Washington, Washington 98195, United States
- Sebastian M. Krajewski Department of Chemistry, University of Washington, Washington 98195, United States

Dylan Rogers – Department of Chemistry, University of Washington, Washington 98195, United States

Werner Kaminsky — Department of Chemistry, University of Washington, Washington 98195, United States;
orcid.org/0000-0002-9100-4909

Complete contact information is available at: https://pubs.acs.org/10.1021/jacs.2c07033

Author Contributions

[†]B.S.M. and A.C. contributed equally to this work

Notes

The authors declare no competing financial interest.

ACKNOWLEDGMENTS

This work was supported by the National Science Foundation (NSF) through a Faculty Early Career Development Program Award (1944843) and by the Research Corporation for Science Advancement through a Cottrell Scholars Award. The X-ray crystallography facility was funded through NSF Grant 0840520. B.S.M. is grateful for support from the NSF Graduate Research Fellowship Program. Prof. Ian Tonks and Prof. Xiaosong Li are acknowledged for insightful discussions on catalytic studies and computational investigations, respectively. The authors thank P. Gannon (UW Chemistry) for additional assistance with X-ray diffraction measurements.

REFERENCES

- (1) Tauster, S. J. Strong Metal-Support Interactions. Acc. Chem. Res. 1987, 20, 389–394.
- (2) Campbell, C. T. Catalyst-Support Interactions: Electronic Perturbations. *Nat. Chem.* **2012**, *4*, 597–598.
- (3) Bruix, A.; Rodriguez, J. A.; Ramírez, P. J.; Senanayake, S. D.; Evans, J.; Park, J. B.; Stacchiola, D.; Liu, P.; Hrbek, J.; Illas, F. A New Type of Strong Metal—Support Interaction and the Production of H₂ through the Transformation of Water on Pt/CeO₂(111) and Pt/CeO₂/TiO₂(110) Catalysts. *J. Am. Chem. Soc.* **2012**, *134*, 8968–8974.
- (4) van Deelen, T. W.; Mejía, C. H.; de Jong, K. P. Control of Metal-Support Interactions in Heterogeneous Catalysts to Enhance Activity and Selectivity. *Nat. Catal.* **2019**, *2*, 955–970.
- (5) Liu, L.; Corma, A. Metal Catalysts for Heterogeneous Catalysis: From Single Atoms to Nanoclusters and Nanoparticles. *Chem. Rev.* **2018**, *118*, 4981–5079.
- (6) Qi, K.; Chhowalla, M.; Voiry, D. Single Atom Is Not Alone: Metal—Support Interactions in Single-Atom Catalysis. *Mater. Today* **2020**, *40*, 173–192.
- (7) Wang, A.; Li, J.; Zhang, T. Heterogeneous Single-Atom Catalysis. *Nat. Rev. Chem.* **2018**, *2*, 65–81.
- (8) Wang, X.; Zhang, Y.; Wu, J.; Zhang, Z.; Liao, Q.; Kang, Z.; Zhang, Y. Single-Atom Engineering to Ignite 2D Transition Metal Dichalcogenide Based Catalysis: Fundamentals, Progress, and Beyond. *Chem. Rev.* **2022**, *122*, 1273–1348.
- (9) Lou, Y.; Zheng, Y.; Li, X.; Ta, N.; Xu, J.; Nie, Y.; Cho, K.; Liu, J. Pocketlike Active Site of Rh₁/MoS₂ Single-Atom Catalyst for Selective Crotonaldehyde Hydrogenation. *J. Am. Chem. Soc.* **2019**, *141*, 19289–19295.
- (10) Hong, W.; Meza, E.; Li, C. W. Controlling the Co-S Coordination Environment in Co-Doped WS₂ Nanosheets for

- Electrochemical Oxygen Reduction. J. Mater. Chem. A 2021, 9, 19865–19873.
- (11) Chhowalla, M.; Shin, H. S.; Eda, G.; Li, L.-J.; Loh, K. P.; Zhang, H. The Chemistry of Two-Dimensional Layered Transition Metal Dichalcogenide Nanosheets. *Nat. Chem.* **2013**, *5*, 263–275.
- (12) Harris, S.; Chianelli, R. R. Catalysis by Transition Metal Sulfides: A Theoretical and Experimental Study of the Relation between the Synergic Systems and the Binary Transition Metal Sulfides. *J. Catal.* **1986**, *98*, 17–31.
- (13) Raybaud, P.; Hafner, J.; Kresse, G.; Kasztelan, S.; Toulhoat, H. Structure, Energetics, and Electronic Properties of the Surface of a Promoted MoS₂ Catalyst: An Ab Initio Local Density Functional Study. *J. Catal.* **2000**, *190*, 128–143.
- (14) Berhault, G.; Lacroix, M.; Breysse, M.; Maugé, F.; Lavalley, J.-C.; Nie, H.; Qu, L. Characterization of Acidic Sites of Silica-Supported Transition Metal Sulfides by Pyridine and 2,6 Dimethylpyridine Adsorption: Relation to Activity in CH₃SH Condensation. *J. Catal.* **1998**, *178*, 555–565.
- (15) Bolar, S.; Shit, S.; Murmu, N. C.; Samanta, P.; Kuila, T. Activation Strategy of MoS₂ as HER Electrocatalyst through Doping-Induced Lattice Strain, Band Gap Engineering, and Active Crystal Plane Design. ACS Appl. Mater. Interfaces 2021, 13, 765–780.
- (16) Jaramillo, T. F.; Jørgensen, K. P.; Bonde, J.; Nielsen, J. H.; Horch, S.; Chorkendorff, I. Identification of Active Edge Sites for Electrochemical H₂ Evolution from MoS₂ Nanocatalysts. *Science* **2007**, 317, 100–102.
- (17) Bonde, J.; Moses, P. G.; Jaramillo, T. F.; Nørskov, J. K.; Chorkendorff, I. Hydrogen Evolution on Nano-Particulate Transition Metal Sulfides. *Faraday Discuss.* **2009**, *140*, 219–231.
- (18) Tuxen, A. K.; Füchtbauer, H. G.; Temel, B.; Hinnemann, B.; Topsøe, H.; Knudsen, K. G.; Besenbacher, F.; Lauritsen, J. V. Atomic-Scale Insight into Adsorption of Sterically Hindered Dibenzothiophenes on MoS₂ and Co–Mo–S Hydrotreating Catalysts. *J. Catal.* **2012**, 295, 146–154.
- (19) Lauritsen, J. V.; Nyberg, M.; Nørskov, J. K.; Clausen, B. S.; Topsøe, H.; Lægsgaard, E.; Besenbacher, F. Hydrodesulfurization Reaction Pathways on MoS₂ Nanoclusters Revealed by Scanning Tunneling Microscopy. *J. Catal.* **2004**, 224, 94–106.
- (20) Lauritsen, J. V.; Kibsgaard, J.; Olesen, G. H.; Moses, P. G.; Hinnemann, B.; Helveg, S.; Nørskov, J. K.; Clausen, B. S.; Topsøe, H.; Lægsgaard, E.; Besenbacher, F. Location and Coordination of Promoter Atoms in Co- and Ni-Promoted MoS₂-Based Hydrotreating Catalysts. *J. Catal.* **2007**, 249, 220–233.
- (21) Kibsgaard, J.; Tuxen, A.; Knudsen, K. G.; Brorson, M.; Topsøe, H.; Lægsgaard, E.; Lauritsen, J. V.; Besenbacher, F. Comparative Atomic-Scale Analysis of Promotional Effects by Late 3d-Transition Metals in MoS₂ Hydrotreating Catalysts. *J. Catal.* **2010**, 272, 195–203.
- (22) Tuxen, A.; Kibsgaard, J.; Gøbel, H.; Lægsgaard, E.; Topsøe, H.; Lauritsen, J. V.; Besenbacher, F. Size Threshold in the Dibenzothiophene Adsorption on MoS_2 Nanoclusters. *ACS Nano* **2010**, *4*, 4677–4682.
- (23) Rangarajan, S.; Mavrikakis, M. On the Preferred Active Sites of Promoted MoS_2 for Hydrodesulfurization with Minimal Organonitrogen Inhibition. *ACS Catal.* **2017**, *7*, 501–509.
- (24) Mom, R. V.; Louwen, J. N.; Frenken, J. W. M.; Groot, I. M. N. In Situ Observations of an Active MoS₂ Model Hydrodesulfurization Catalyst. *Nat. Commun.* **2019**, *10*, 2546.
- (25) Chirik, P. J.; Wieghardt, K. Radical Ligands Confer Nobility on Base-Metal Catalysts. *Science* **2010**, 327, 794–795.
- (26) Praneeth, V. K. K.; Ringenberg, M. R.; Ward, T. R. Redox-Active Ligands in Catalysis. *Angew. Chem., Int. Ed.* **2012**, *51*, 10228–10234.
- (27) Eisenhart, R. J.; Clouston, L. J.; Lu, C. C. Configuring Bonds between First-Row Transition Metals. Acc. Chem. Res. 2015, 48, 2885–2894.
- (28) Cammarota, R. C.; Clouston, L. J.; Lu, C. C. Leveraging Molecular Metal–Support Interactions for H_2 and N_2 Activation. Coord. Chem. Rev. 2017, 334, 100–111.

- (29) Bosnich, B. Cooperative Bimetallic Redox Reactivity. *Inorg. Chem.* **1999**, 38, 2554–2562.
- (30) Tyo, E. C.; Vajda, S. Catalysis by Clusters with Precise Numbers of Atoms. *Nat. Nanotechnol.* **2015**, *10*, 577–588.
- (31) Du, X.; Jin, R. Atomically Precise Metal Nanoclusters for Catalysis. ACS Nano 2019, 13, 7383-7387.
- (32) Reed, C. J.; Agapie, T. A Terminal Fe^{III}—Oxo in a Tetranuclear Cluster: Effects of Distal Metal Centers on Structure and Reactivity. *J. Am. Chem. Soc.* **2019**, *141*, 9479—9484.
- (33) Carr, C. R.; Taheri, A.; Berben, L. A. Fast Proton Transfer and Hydrogen Evolution Reactivity Mediated by $[Co_{13}C_2(CO)_{24}]^{4-}$. *J. Am. Chem. Soc.* **2020**, *142*, 12299–12305.
- (34) McSkimming, A.; Suess, D. L. M. Dinitrogen Binding and Activation at a Molybdenum–Iron–Sulfur Cluster. *Nat. Chem.* **2021**, 13, 666–670.
- (35) Amtawong, J.; Balcells, D.; Wilcoxen, J.; Handford, R. C.; Biggins, N.; Nguyen, A. I.; Britt, R. D.; Tilley, T. D. Isolation and Study of Ruthenium—Cobalt Oxo Cubanes Bearing a High-Valent, Terminal RuV—Oxo with Significant Oxyl Radical Character. *J. Am. Chem. Soc.* **2019**, *141*, 19859—19869.
- (36) Schreiber, E.; Fertig, A. A.; Brennessel, W. W.; Matson, E. M. Oxygen-Atom Defect Formation in Polyoxovanadate Clusters via Proton-Coupled Electron Transfer. *J. Am. Chem. Soc.* **2022**, *144*, 5029–5041.
- (37) Li, G.; Jin, R. Atomically Precise Gold Nanoclusters as New Model Catalysts. *Acc. Chem. Res.* **2013**, *46*, 1749–1758.
- (38) Zhu, Y.; Qian, H.; Jin, R. An Atomic-Level Strategy for Unraveling Gold Nanocatalysis from the Perspective of Au_n(SR)_m Nanoclusters. *Chem. Eur. J.* **2010**, *16*, 11455–11462.
- (39) Liu, Y.; Tsunoyama, H.; Akita, T.; Xie, S.; Tsukuda, T. Aerobic Oxidation of Cyclohexane Catalyzed by Size-Controlled Au Clusters on Hydroxyapatite: Size Effect in the Sub-2 nm Regime. *ACS Catal.* **2011**, *1*, 2–6.
- (40) Chen, W.; Chen, S. Oxygen Electroreduction Catalyzed by Gold Nanoclusters: Strong Core Size Effects. *Angew. Chem., Int. Ed.* **2009**, *121*, 4450–4453.
- (41) Jin, R.; Li, G.; Sharma, S.; Li, Y.; Du, X. Toward Active-Site Tailoring in Heterogeneous Catalysis by Atomically Precise Metal Nanoclusters with Crystallographic Structures. *Chem. Rev.* **2021**, *121*, 567–648.
- (42) Kephart, J. A.; Mitchell, B. S.; Chirila, A.; Anderton, K. J.; Rogers, D.; Kaminsky, W.; Velian, A. Atomically Defined Nanopropeller Fe₃Co₆Se₈(Ph₂PNTol)₆: Functional Model for the Electronic Metal–Support Interaction Effect and High Catalytic Activity for Carbodiimide Formation. *J. Am. Chem. Soc.* **2019**, *141*, 19605–19610.
- (43) Kephart, J. A.; Romero, C. G.; Tseng, C.-C.; Anderton, K. J.; Yankowitz, M.; Kaminsky, W.; Velian, A. Hierarchical Nanosheets Built from Superatomic Clusters: Properties, Exfoliation and Single-Crystal-to-Single-Crystal Intercalation. *Chem. Sci.* **2020**, *11*, 10744–10751.
- (44) Mitchell, B. S.; Krajewski, S. M.; Kephart, J. A.; Rogers, D.; Kaminsky, W.; Velian, A. Redox-Switchable Allosteric Effects in Molecular Clusters. *JACS Au* **2022**, *2*, 92–96.
- (45) Kephart, J. A.; Mitchell, B. S.; Kaminsky, W.; Velian, A. Multi-Active Site Dynamics on a Molecular Cr/Co/Se Cluster Catalyst. *J. Am. Chem. Soc.* **2022**, *144*, 9206–9211.
- (46) Mitchell, B. S.; Kaminsky, W.; Velian, A. Tuning the Electronic Structure of Atomically Precise Sn/Co/Se Nanoclusters via Redox Matching of Tin(IV) Surface Sites. *Inorg. Chem.* **2021**, *60*, 6135–6139.
- (47) Jin, S.; Venkataraman, D.; DiSalvo, F. J. Ligand Substitution Reactions of $W_6S_8L_6$ with Tricyclohexylphosphine (L = 4-Tert-Butylpyridine or n-Butylamine): ^{31}P NMR and Structural Studies of $W_6S_8(PCy_3)_n(4-Tert-Butylpyridine)_{6-n}$ (0 < n \leq 6) Complexes. *Inorg. Chem.* **2000**, 39, 2747–2757.
- (48) Eames, E. V.; Betley, T. A. Site-Isolated Redox Reactivity in a Trinuclear Iron Complex. *Inorg. Chem.* **2012**, *51*, 10274–10278.

- (49) Champsaur, A. M.; Velian, A.; Paley, D. W.; Choi, B.; Roy, X.; Steigerwald, M. L.; Nuckolls, C. Building Diatomic and Triatomic Superatom Molecules. *Nano Lett.* **2016**, *16*, 5273–5277.
- (50) Petel, B. E.; Brennessel, W. W.; Matson, E. M. Oxygen-Atom Vacancy Formation at Polyoxovanadate Clusters: Homogeneous Models for Reducible Metal Oxides. *J. Am. Chem. Soc.* **2018**, *140*, 8424–8428.
- (51) Venkateswara Rao, P.; Holm, R. H. Synthetic Analogues of the Active Sites of Iron–Sulfur Proteins. *Chem. Rev.* **2004**, *104*, 527–560.
- (52) McSkimming, A.; Suess, D. L. M. Selective Synthesis of Site-Differentiated Fe_4S_4 and Fe_6S_6 Clusters. *Inorg. Chem.* **2018**, *57*, 14904–14912.
- (53) Kephart, J. A.; Boggiano, A. C.; Kaminsky, W.; Velian, A. Inorganic Clusters as Metalloligands: Ligand Effects on the Synthesis and Properties of Ternary Nanopropeller Clusters. *Dalton Trans.* **2020**, *49*, 16464–16473.
- (54) Driver, T. G. Recent Advances in Transition Metal-Catalyzed N-Atom Transfer Reactions of Azides. *Org. Biomol. Chem.* **2010**, *8*, 3831–3846.
- (55) Roizen, J. L.; Harvey, M. E.; Du Bois, J. Metal-Catalyzed Nitrogen-Atom Transfer Methods for the Oxidation of Aliphatic C–H Bonds. *Acc. Chem. Res.* **2012**, *45*, 911–922.
- (56) Wigley, D. E. Organoimido Complexes of the Transition Metals. In *Progress in Inorganic Chemistry*; John Wiley & Sons, Ltd, 1994; pp 239–482.
- (57) Cowley, R. E.; Golder, M. R.; Eckert, N. A.; Al-Afyouni, M. H.; Holland, P. L. Mechanism of Catalytic Nitrene Transfer Using Iron(I)—Isocyanide Complexes. *Organometallics* **2013**, 32, 5289—5298.
- (58) Yousif, M.; Tjapkes, D. J.; Lord, R. L.; Groysman, S. Catalytic Formation of Asymmetric Carbodiimides at Mononuclear Chromium(II/IV) Bis(Alkoxide) Complexes. *Organometallics* **2015**, 34, 5119–5128.
- (59) Choi, B.; Yu, J.; Paley, D. W.; Trinh, M. T.; Paley, M. V.; Karch, J. M.; Crowther, A. C.; Lee, C.-H.; Lalancette, R. A.; Zhu, X.; Kim, P.; Steigerwald, M. L.; Nuckolls, C.; Roy, X. Van Der Waals Solids from Self-Assembled Nanoscale Building Blocks. *Nano Lett.* **2016**, *16*, 1445–1449.
- (60) Bruno, I. J.; Cole, J. C.; Edgington, P. R.; Kessler, M.; Macrae, C. F.; McCabe, P.; Pearson, J.; Taylor, R. New Software for Searching the Cambridge Structural Database and Visualizing Crystal Structures. *Acta Crystallogr., Sect. B: Struct. Sci.* **2002**, *58*, 389–397.
- (61) Groom, C. R.; Bruno, I. J.; Lightfoot, M. P.; Ward, S. C. The Cambridge Structural Database. *Acta Crystallogr., Sect. B: Struct. Sci., Cryst. Eng. Mater.* **2016**, *72*, 171–179.
- (62) A Search for All M...Se Single Bond Lengths in the Cambridge Structural Database (Accessed 2/11/22) Yielded 82 Hits for Cr...Se with a Mean of 2.482 Å and a Standard Deviation of 0.072 Å, 173 Hits for Mn...Se with a Mean of 2.544 Å and a Standard Deviation of 0.104 Å, 591 Hits for Fe...Se with a Mean of 2.389 Å and a Standard Deviation of 0.057 Å, 182 Hits for Co...Se with a Mean of 2.359 Å and a Standard Deviation of 0.062 Å, 237 Hits for Ni...Se with a Mean of 2.350 Å and a Standard Deviation of 0.080 Å, 467 Hits for Cu...Se with a Mean of 2.464 Å with a Standard Deviation of 0.120 Å, and 140 Hits for Zn...Se with a Mean of 2.469 Å with a Standard Deviation of 0.074 Å.
- (63) Evans, D. F. The Determination of the Paramagnetic Susceptibility of Substances in Solution by Nuclear Magnetic Resonance. J. Chem. Soc. 1959, 2003–2005.
- (64) Pinkard, A.; Champsaur, A. M.; Roy, X. Molecular Clusters: Nanoscale Building Blocks for Solid-State Materials. *Acc. Chem. Res.* **2018**, *51*, 919–929.
- (65) Ganguly, S.; Ghosh, A. Seven Clues to Ligand Noninnocence: The Metallocorrole Paradigm. Acc. Chem. Res. 2019, 52, 2003–2014.
- (66) Köhler, F. H. Paramagnetic Complexes in Solution: The NMR Approach. In Encyclopedia of Magnetic Resonance; John Wiley & Sons, Ltd: Chichester, U.K., 2011.
- (67) Luca, O. R.; Konezny, S. J.; Paulson, E. K.; Habib, F.; Luthy, K. M.; Murugesu, M.; Crabtree, R. H.; Batista, V. S. Study of an S = 1

- Ni^{II} Pincer Electrocatalyst Precursor for Aqueous Hydrogen Production Based on Paramagnetic ¹H NMR. *Dalton Trans.* **2013**, 42, 8802.
- (68) Roquette, P.; Maronna, A.; Reinmuth, M.; Kaifer, E.; Enders, M.; Himmel, H.-J. Combining NMR of Dynamic and Paramagnetic Molecules: Fluxional High-Spin Nickel(II) Complexes Bearing Bisguanidine Ligands. *Inorg. Chem.* **2011**, *50*, 1942–1955.
- (69) Frisch, M. J.; Trucks, G. W.; Schlegel, H. B.; Scuseria, G. E.; Robb, M. A.; Cheeseman, J. R.; Scalmani, G.; Barone, V.; Petersson, G. A.; Nakatsuji, H.; Li, X.; Caricato, M.; Marenich, A. V.; Bloino, J.; Janesko, B. G.; Gomperts, R.; Mennucci, B.; Hratchian, H. P.; Ortiz, J. V.; Izmaylov, A. F.; Sonnenberg, J. L.; Williams-Young, D.; Ding, F.; Lipparini, F.; Egidi, F.; Goings, J.; Peng, B.; Petrone, A.; Henderson, T.; Ranasinghe, D.; Zakrzewski, V. G.; Gao, J.; Rega, N.; Zheng, G.; Liang, W.; Hada, M.; Ehara, M.; Toyota, K.; Fukuda, R.; Hasegawa, J.; Ishida, M.; Nakajima, T.; Honda, Y.; Kitao, O.; Nakai, H.; Vreven, T.; Throssell, K.; Montgomery, J. A., Jr.; Peralta, J. E.; Ogliaro, F.; Bearpark, M. J.; Heyd, J. J.; Brothers, E. N.; Kudin, K. N.; Staroverov, V. N.; Keith, T. A.; Kobayashi, R.; Normand, J.; Raghavachari, K.; Rendell, A. P.; Burant, J. C.; Iyengar, S. S.; Tomasi, J.; Cossi, M.; Millam, J. M.; Klene, M.; Adamo, C.; Cammi, R.; Ochterski, J. W.; Martin, R. L.; Morokuma, K.; Farkas, O.; Foresman, J. B.; Fox, D. J. Gaussian 16 Rev. A.03; Gaussian, Inc.: Wallingford, CT, 2016.
- (70) Becke, A. D. Density-functional Thermochemistry. III. The Role of Exact Exchange. *J. Chem. Phys.* **1993**, 98, 5648–5652.
- (71) Stephens, P. J.; Devlin, F. J.; Chabalowski, C. F.; Frisch, M. J. Ab Initio Calculation of Vibrational Absorption and Circular Dichroism Spectra Using Density Functional Force Fields. *J. Phys. Chem.* **1994**, *98*, 11623–11627.
- (72) Kendall, R. A.; Dunning, T. H.; Harrison, R. J. Electron Affinities of the First-row Atoms Revisited. Systematic Basis Sets and Wave Functions. *J. Chem. Phys.* **1992**, *96*, 6796–6806.
- (73) Lu, T.; Chen, F. Multiwfn: A Multifunctional Wavefunction Analyzer. J. Comput. Chem. 2012, 33, 580-592.
- (74) Wu, M.; Yao, X.; Hao, Y.; Dong, H.; Cheng, Y.; Liu, H.; Lu, F.; Wang, W.; Cho, K.; Wang, W.-H. Electronic Structures, Magnetic Properties and Band Alignments of 3d Transition Metal Atoms Doped Monolayer MoS₂. *Phys. Lett. A* **2018**, 382, 111–115.
- (75) Gangwar, R.; Pandey, D.; Kancharlapalli, S.; Raychaudhuri, D.; Chakrabarti, A.; Banerjee, A.; Ghanty, T. K. Ab Initio Study of Adsorption of Fission Gas Atoms Xe and Kr on MoS₂ Monolayer Functionalized with 3d Transition Metals. *J. Phys. Chem. C* **2021**, *125*, 1493–1508.
- (76) Armentrout, P. B.; Halle, L. F.; Beauchamp, J. L. Periodic Trends in Transition Metal-Hydrogen, Metal-Carbon, and Metal-Oxygen Bond Dissociation Energies. Correlation with Reactivity and Electronic Structure. *J. Am. Chem. Soc.* **1981**, *103*, 6501–6502.
- (77) Edwards, N. Y.; Eikey, R. A.; Loring, M. I.; Abu-Omar, M. M. High-Valent Imido Complexes of Manganese and Chromium Corroles. *Inorg. Chem.* **2005**, *44*, 3700–3708.
- (78) Dong, Y.; Clarke, R. M.; Zheng, S.-L.; Betley, T. A. Synthesis and Electronic Structure Studies of a Cr-Imido Redox Series. *Chem. Commun.* **2020**, *56*, 3163–3166.
- (79) Shi, H.; Xie, J.; Lam, W. W. Y.; Man, W.-L.; Mak, C.-K.; Yiu, S.-M.; Lee, H. K.; Lau, T.-C. Generation and Reactivity of a One-Electron-Oxidized Manganese(V) Imido Complex with a Tetraamido Macrocyclic Ligand. *Chem. Eur. J.* **2019**, *25*, 12895–12899.
- (80) Zdilla, M. J.; Abu-Omar, M. M. Mechanism of Catalytic Aziridination with Manganese Corrole: The Often Postulated High-Valent Mn(V) Imido Is Not the Group Transfer Reagent. *J. Am. Chem. Soc.* **2006**, *128*, 16971–16979.
- (81) King, E. R.; Hennessy, E. T.; Betley, T. A. Catalytic C—H Bond Amination from High-Spin Iron Imido Complexes. *J. Am. Chem. Soc.* **2011**, *133*, 4917–4923.
- (82) Iovan, D. A.; Betley, T. A. Characterization of Iron-Imido Species Relevant for N-Group Transfer Chemistry. *J. Am. Chem. Soc.* **2016**, 138, 1983–1993.
- (83) Cowley, R. E.; Eckert, N. A.; Vaddadi, S.; Figg, T. M.; Cundari, T. R.; Holland, P. L. Selectivity and Mechanism of Hydrogen Atom

- Transfer by an Isolable Imidoiron(III) Complex. J. Am. Chem. Soc. 2011, 133, 9796–9811.
- (84) Cowley, R. E.; Holland, P. L. Ligand Effects on Hydrogen Atom Transfer from Hydrocarbons to Three-Coordinate Iron Imides. *Inorg. Chem.* **2012**, *51*, 8352–8361.
- (8Š) Goswami, M.; Lyaskovskyy, V.; Domingos, S. R.; Buma, W. J.; Woutersen, S.; Troeppner, O.; Ivanović-Burmazović, I.; Lu, H.; Cui, X.; Zhang, X. P.; Reijerse, E. J.; DeBeer, S.; van Schooneveld, M. M.; Pfaff, F. F.; Ray, K.; de Bruin, B. Characterization of Porphyrin-Co(III)-'Nitrene Radical' Species Relevant in Catalytic Nitrene Transfer Reactions. J. Am. Chem. Soc. 2015, 137, 5468–5479.
- (86) Gu, Z.-Y.; Liu, Y.; Wang, F.; Bao, X.; Wang, S.-Y.; Ji, S.-J. Cobalt(II)-Catalyzed Synthesis of Sulfonyl Guanidines via Nitrene Radical Coupling with Isonitriles: A Combined Experimental and Computational Study. *ACS Catal.* **2017**, *7*, 3893–3899.
- (87) Baek, Y.; Betley, T. A. Catalytic C-H Amination Mediated by Dipyrrin Cobalt Imidos. *J. Am. Chem. Soc.* **2019**, *141*, 7797–7806.
- (88) Baek, Y.; Das, A.; Zheng, S.-L.; Reibenspies, J. H.; Powers, D. C.; Betley, T. A. C–H Amination Mediated by Cobalt Organoazide Adducts and the Corresponding Cobalt Nitrenoid Intermediates. *J. Am. Chem. Soc.* **2020**, *142*, 11232–11243.
- (89) Dong, Y.; Lukens, J. T.; Clarke, R. M.; Zheng, S.-L.; Lancaster, K. M.; Betley, T. A. Synthesis, Characterization and C—H Amination Reactivity of Nickel Iminyl Complexes. *Chem. Sci.* **2020**, *11*, 1260—1268.
- (90) Dong, Y.; Lund, C. J.; Porter, G. J.; Clarke, R. M.; Zheng, S.-L.; Cundari, T. R.; Betley, T. A. Enantioselective C–H Amination Catalyzed by Nickel Iminyl Complexes Supported by Anionic Bisoxazoline (BOX) Ligands. *J. Am. Chem. Soc.* **2021**, *143*, 817–829.
- (91) Dong, Y.; Clarke, R. M.; Porter, G. J.; Betley, T. A. Efficient C—H Amination Catalysis Using Nickel-Dipyrrin Complexes. *J. Am. Chem. Soc.* **2020**, *142*, 10996—11005.
- (92) Bagchi, V.; Paraskevopoulou, P.; Das, P.; Chi, L.; Wang, Q.; Choudhury, A.; Mathieson, J. S.; Cronin, L.; Pardue, D. B.; Cundari, T. R.; Mitrikas, G.; Sanakis, Y.; Stavropoulos, P. A Versatile Tripodal Cu(I) Reagent for C–N Bond Construction via Nitrene-Transfer Chemistry: Catalytic Perspectives and Mechanistic Insights on C–H Aminations/Amidinations and Olefin Aziridinations. *J. Am. Chem. Soc.* **2014**, *136*, 11362–11381.
- (93) Carsch, K. M.; DiMucci, I. M.; Iovan, D. A.; Li, A.; Zheng, S.-L.; Titus, C. J.; Lee, S. J.; Irwin, K. D.; Nordlund, D.; Lancaster, K. M.; Betley, T. A. Synthesis of a Copper-Supported Triplet Nitrene Complex Pertinent to Copper-Catalyzed Amination. *Science* **2019**, 365, 1138–1143.
- (94) Kuijpers, P. F.; van der Vlugt, J. I.; Schneider, S.; de Bruin, B. Nitrene Radical Intermediates in Catalytic Synthesis. *Chem. Eur. J.* **2017**, 23, 13819–13829.
- (95) Baek, Y.; Betley, T. A. Reversible C–C Bond Cleavage of a Cobalt Diketimide into an Elusive Cobalt Aryl Nitrenoid Complex. *Angew. Chem., Int. Ed.* **2022**, *61*, No. e202115437.
- (96) Wilding, M. J. T.; Iovan, D. A.; Wrobel, A. T.; Lukens, J. T.; MacMillan, S. N.; Lancaster, K. M.; Betley, T. A. Direct Comparison of C–H Bond Amination Efficacy through Manipulation of Nitrogen-Valence Centered Redox: Imido versus Iminyl. *J. Am. Chem. Soc.* **2017**, 139, 14757–14766.
- (97) Crabtree, R. H. The Organometallic Chemistry of the Transition Metals, 4th ed.; Jon Wiley & Sons, Inc, 2005.
- (98) Haber, J.; Mlodnicka, T.; Poltowicz, J. Metal-Dependent Reactivity of Some Metalloporphyrins in Oxidation with Dioxygen. *J. Mol. Catal.* **1989**, *54*, 451–461.
- (99) Feng, X.-T.; Yu, J.-G.; Lei, M.; Fang, W.-H.; Liu, S. Toward Understanding Metal-Binding Specificity of Porphyrin: A Conceptual Density Functional Theory Study. *J. Phys. Chem. B* **2009**, *113*, 13381–13389.